Electronic Supplementary Material (ESI) for Materials Horizons.

Supporting Information for

Anion-induced Electronic Localization and Polarized Cobalt Clusters for Highly-efficient Water Splitting

Yucheng Wu, Yanli Yu, Wei Shen, Yimin Jiang, Rongxing He, Ming Li**

Key Laboratory of Luminescence Analysis and Molecular Sensing (Southwest University), Ministry of Education, College of Chemistry and Chemical Engineering, Southwest University, Chongqing 400715, P. R. China

*Corresponding author: E-mail address, herx@swu.edu.cn (R. He), liming@swu.edu.cn (M. Li).

Theoretical calculations

Density functional theory (DFT) calculations were performed within the Vienna Ab initio Simulation Package (VASP)[1, 2]. The interaction between core electrons and ions was described by a projector truncated wave (PAW) with a truncation energy of 400 eV, and the *k* point in the Brillouin region was set to 3×3×1. The generalized gradient approximation (GGA) functional of Perdew-Burke-Ernzerhof (PBE) functional was applied as the exchange-correlation functional. The vacuum layer in the z-axis direction was set to 15 Å to avoid the interaction between periodical images. In the calculation process, the convergence standard of energy and force were 10^{-5} eV and 0.02 eV $Å^{-1}$, respectively. Based on previous work[3-6], Graphene (001) was used to simulate a small plane of carbon nanotubes. The carbon nanotube with replacing a C atom by a N atom, as a model, served as the nitrogen-doped carbon nanotube. According to previous reports[7, 8], the Co cluster was simulated by multiple Co atoms. Based on the Co NCNTs model, an N atom was adsorbed to the Co cluster to construct the N-Co NCNTs model because Co and N are connected through the Co-N bond. The dimensions of the N-Co NCNTs and Co NCNTs supercell are both 9.840 × 9.840 × 18.40 $Å^3$ and the angles of N-Co NCNTs and Co NCNTs models are both 90 degrees × 90 degrees ×120 degrees. The free energies of H_2, H_2O, and O_2 were collected from previous works[9-11]. The reaction Gibbs free energies of alkaline OER four elementary steps were described as follows:

$$\Delta G_1 = G_{OH^*} + G_{H^+ + e^-} - G_{H_2O(l)} - G_*$$

$$\Delta G_2 = G_{O^*} + G_{H^+ + e^-} - G_{OH^*}$$

$$\Delta G_3 = G_{OOH^*} + G_{H^+ + e^-} - G_{H_2O(l)} - G_{O^*}$$

$$\Delta G_4 = G_{O^*} + G_{O_{2(g)}} + G_{H^+ + e^-} - G_{OOH^*}$$

where * denotes the surface bound species. For HER, the Gibbs free-energy (ΔG_{H^*}) was expressed as: $\Delta G_{H^*} = \Delta E_{H^*} + \Delta ZPE - T\Delta S$, where E_{ZPE} is the zero energy, ΔS is the entropy change, and T is the system temperature (298.15K, in our work).

Figures and Tables:

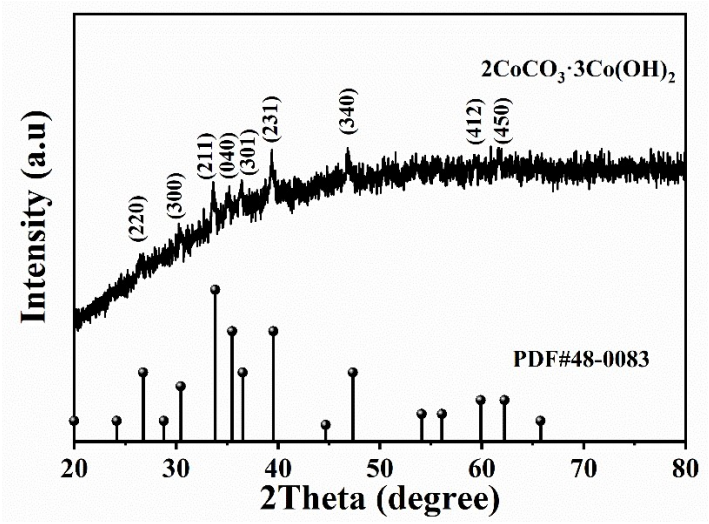

Fig S1. XRD spectra of the Co(II) carbonate hydroxide.

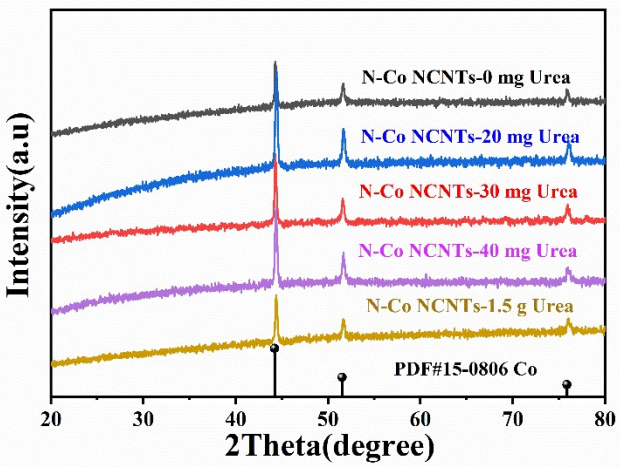

Fig S2. XRD spectra of the catalysts with different amount of urea.

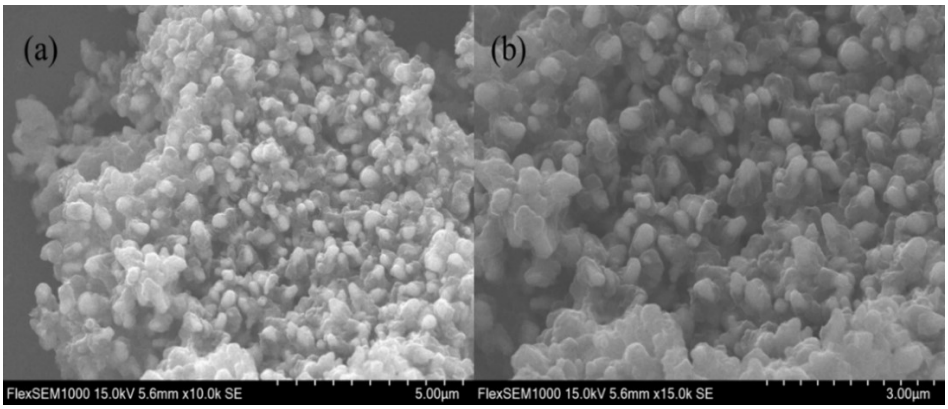

Fig S3. SEM images of Co NCNTs.

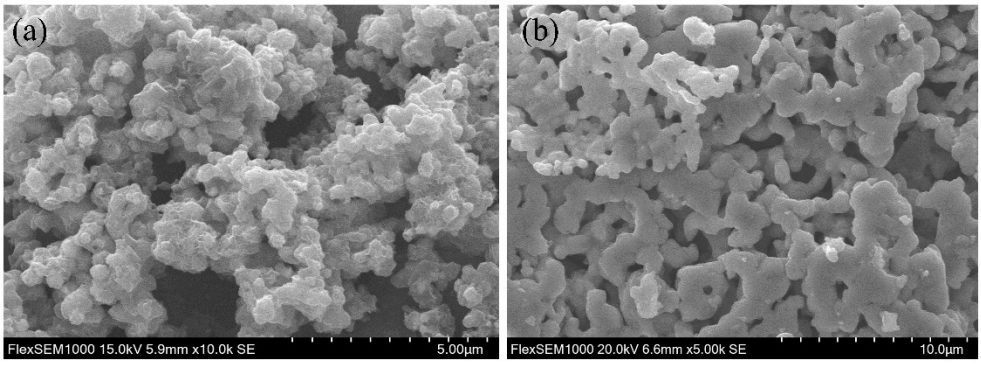

Fig S4. SEM image of N-Co NCNTs obtained at (a) 600 ℃ and (b) 800 ℃.

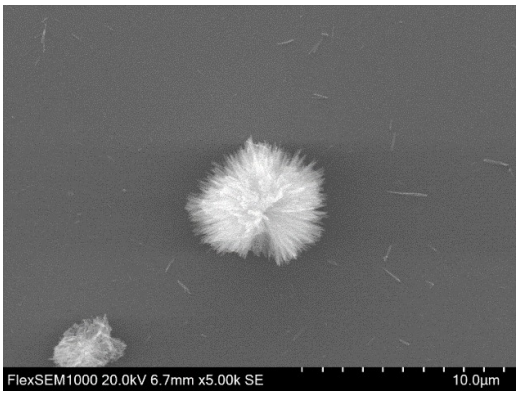

Fig S5. SEM image of sea urchin-like Co (II) carbonate hydroxide.

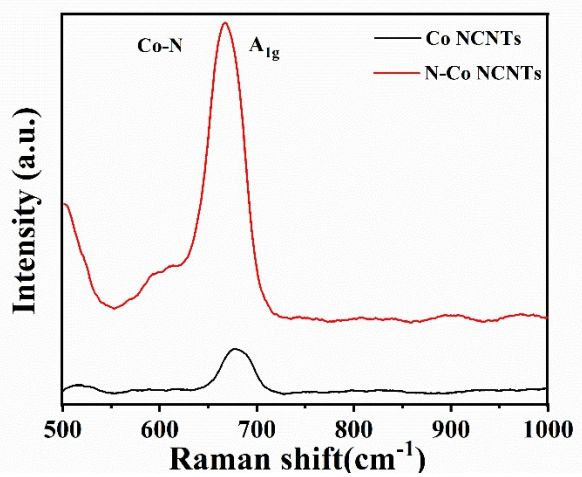

Fig S6. Raman spectra of N-Co NCNTs and Co NCNTs.

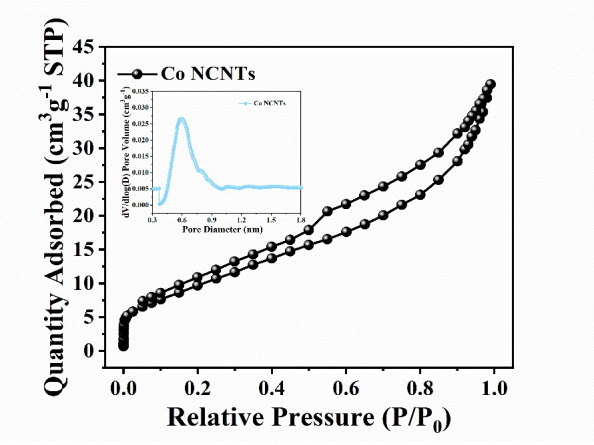

Fig S7. The N_2 adsorption–desorption isotherm and pore-size distribution (inset) of Co NCNTs.

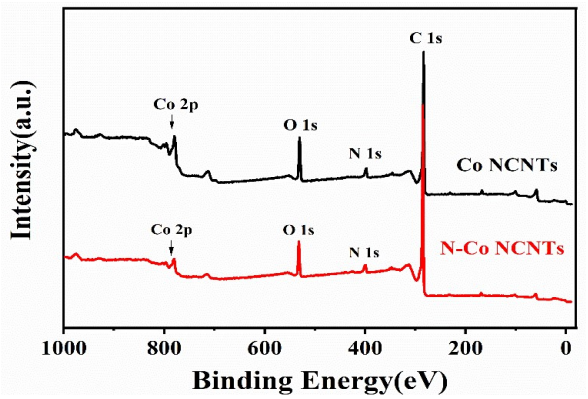

Fig S8. The XPS survey spectrum of N-Co NCNTs and Co NCNTs.

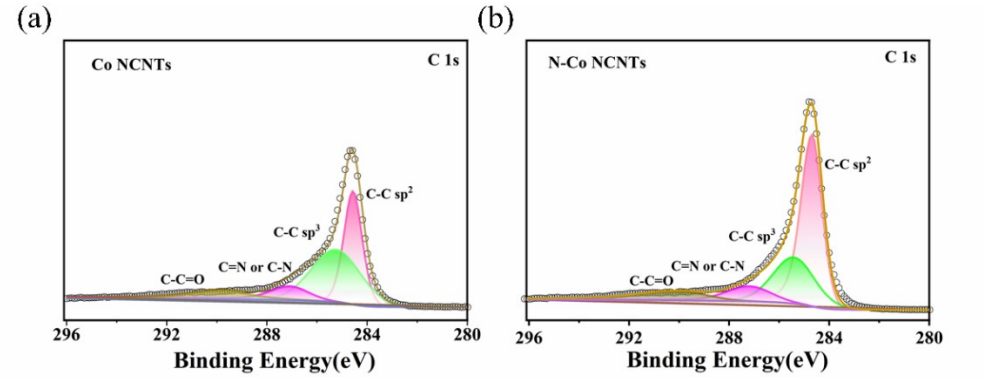

Fig S9. High-resolution C 1s spectra of Co NCNTs and N-Co NCNTs.

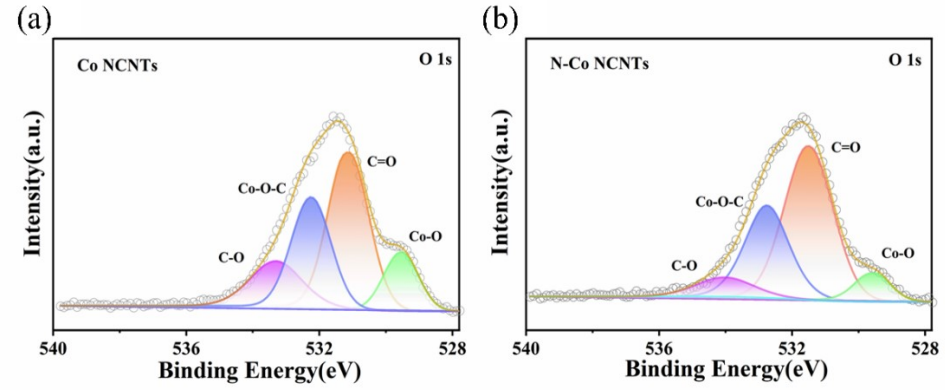

Fig S10. High-resolution O 1s spectra of Co NCNTs and N-Co NCNTs.

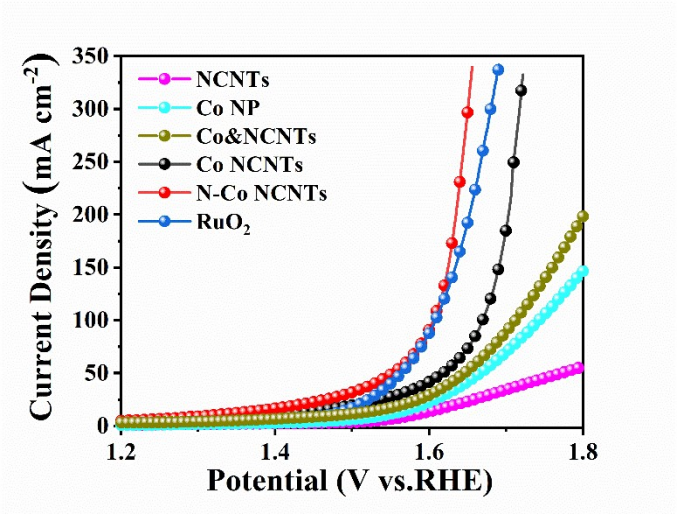

Fig S11. OER polarization curves of N-Co NCNTs, Co NCNTs, Co-NCNTs, Co NP, RuO_2 and NCNTs.

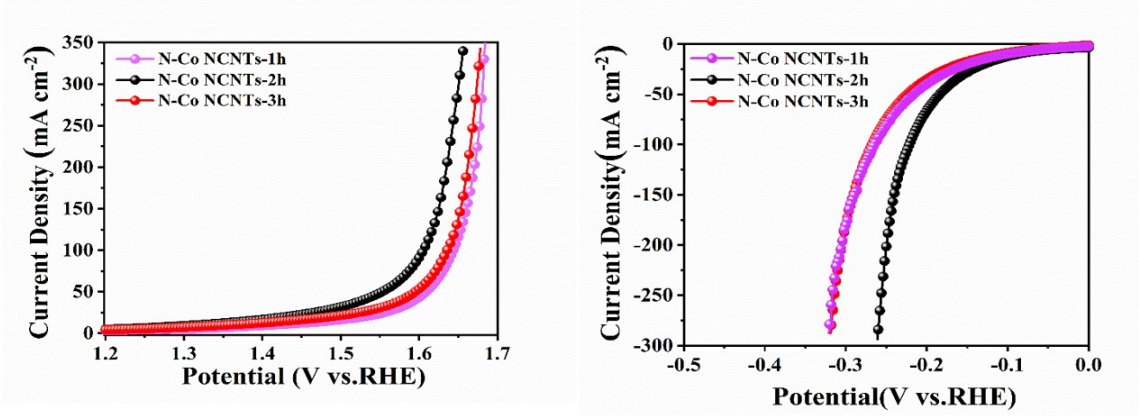

Fig S12. LSV polarization curves of N-Co NCNTs at different annealing times.

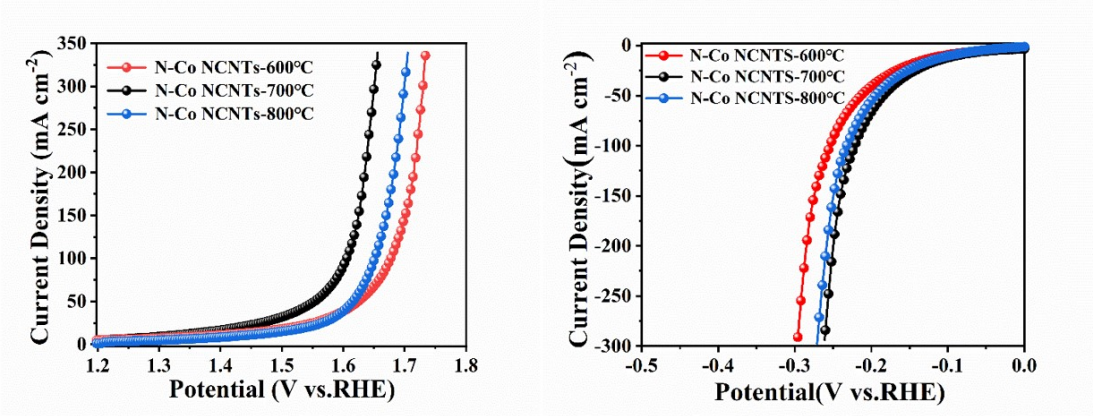

Fig S13. LSV polarization curves of N-Co NCNTs at different annealing temperatures.

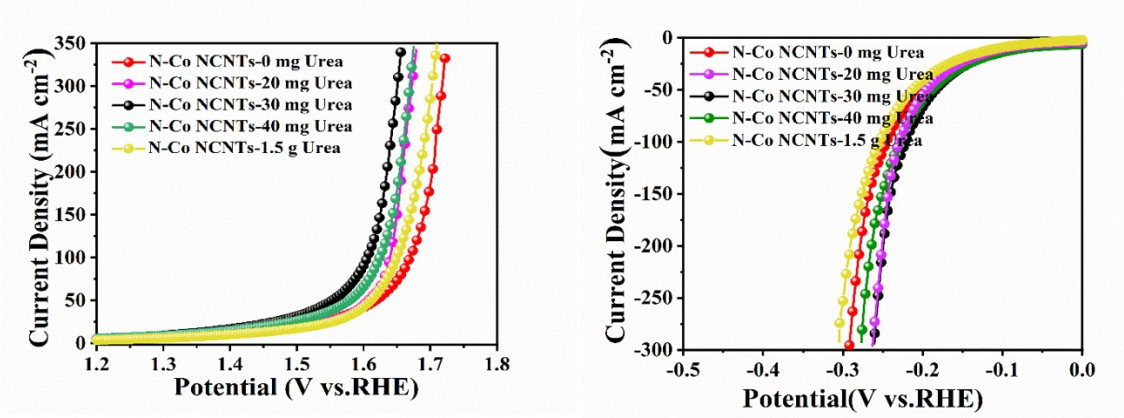

Fig S14. LSV polarization curves of N-Co NCNTs with different amount of urea.

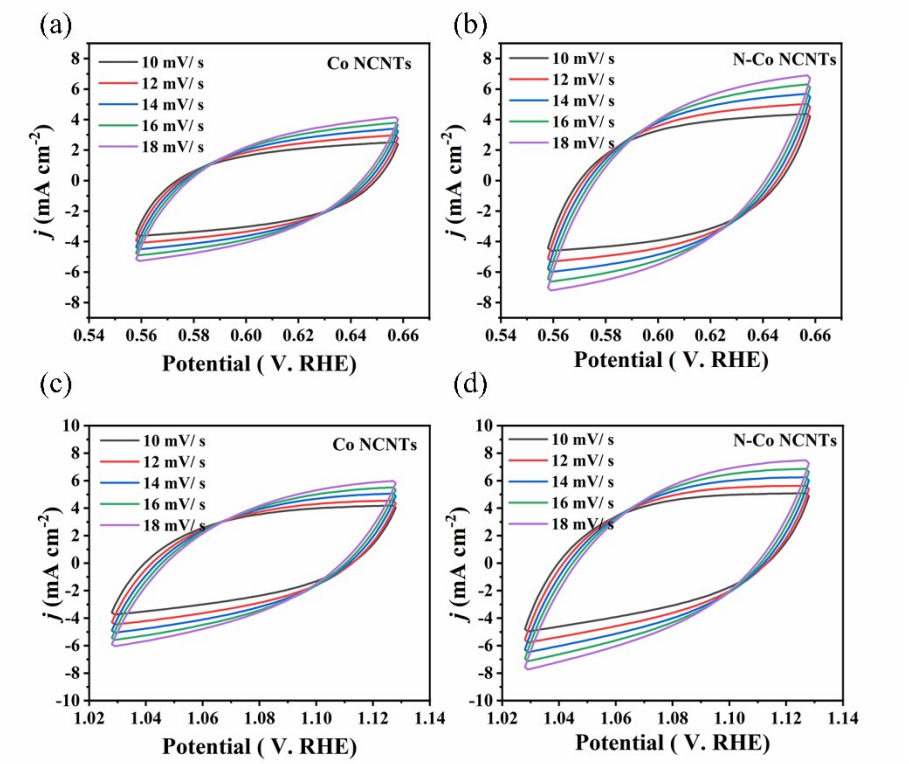

Fig S15. Cyclic voltammetry curves for the HER (a,b) and for the OER (c,d).

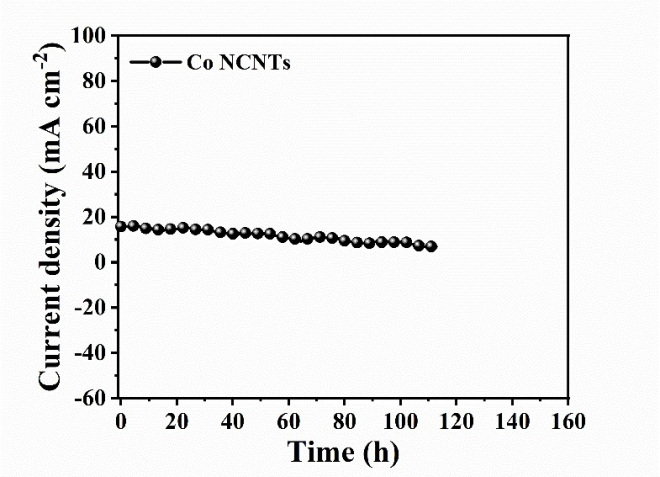

Fig S16. Time-dependent current density curve of Co NCNTs for OER in alkaline solution.

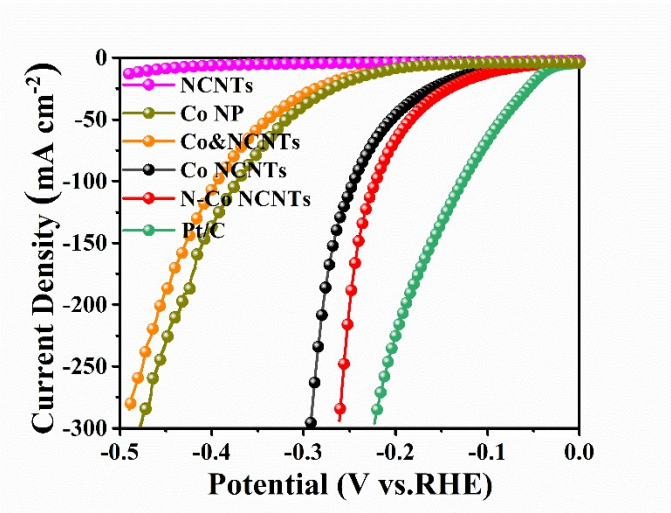

Fig S17. HER polarization curves of N-Co NCNTs, Co NCNTs, Co-NCNTs, Co NP, Pt/C and NCNTs.

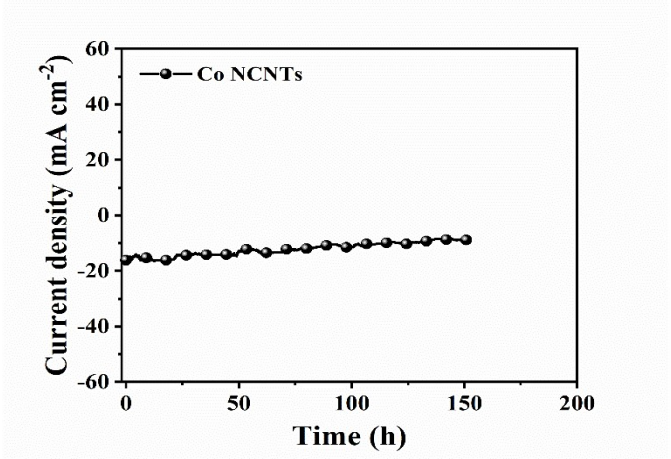

Fig S18. Time-dependent current density curve of Co NCNTs for HER in alkaline solution.

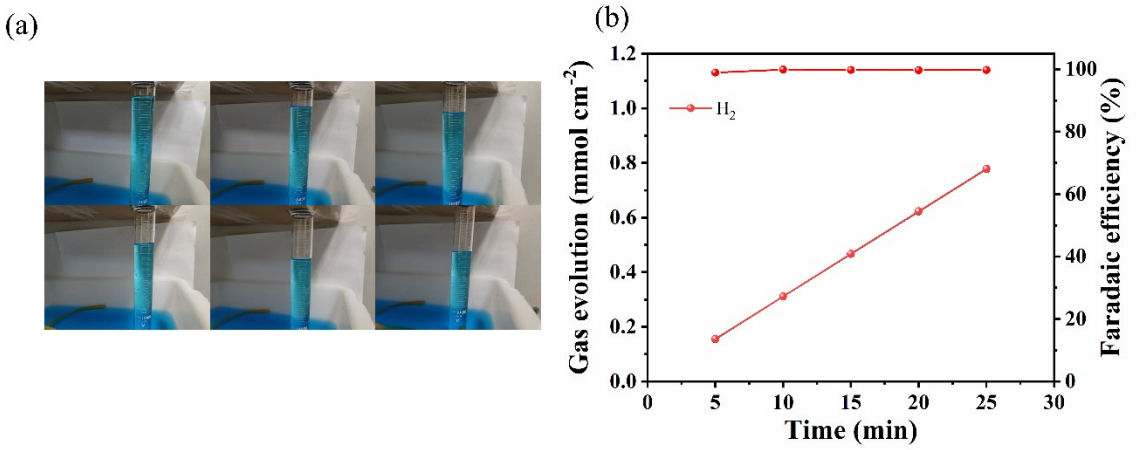

Fig S19. (a) Hydrogen volume for Faraday efficiency experiment of HER. (b) Faraday efficiency of N-Co NCNTs for HER.

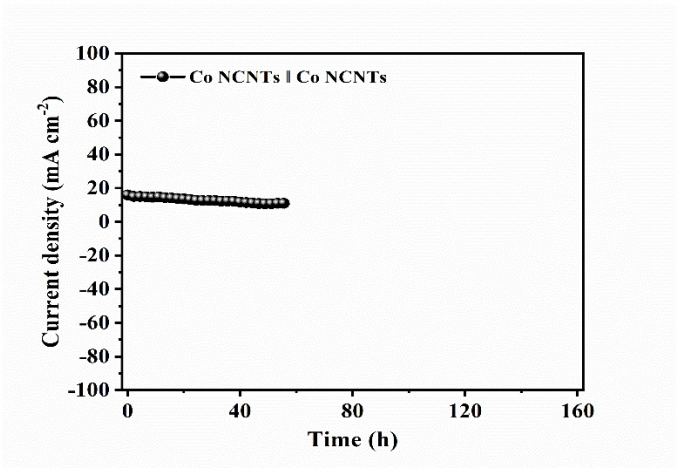

Fig S20. Stability testing of Co-NCNTs.

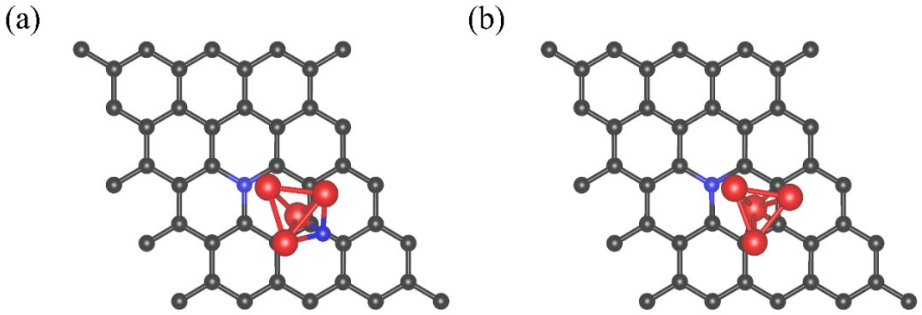

Fig S21. Theoretical models for N-Co NCNTs (a) and Co-NCNTs (b).

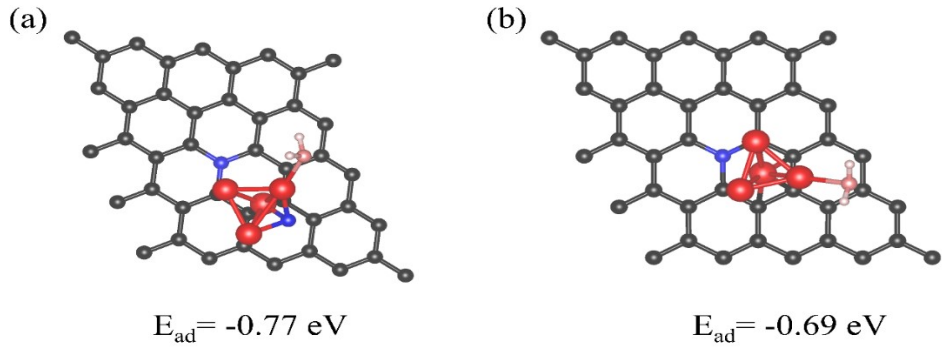

Fig S22. Adsorption energies of H_2O adsorption on N-Co NCNTs (a) and Co NCNTs (b).

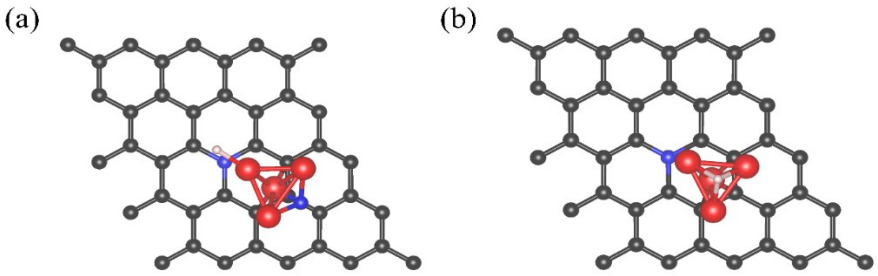

Fig S23. Adsorption model of H^* intermediates of N-Co NCNTs (a) and Co NCNTs (b).

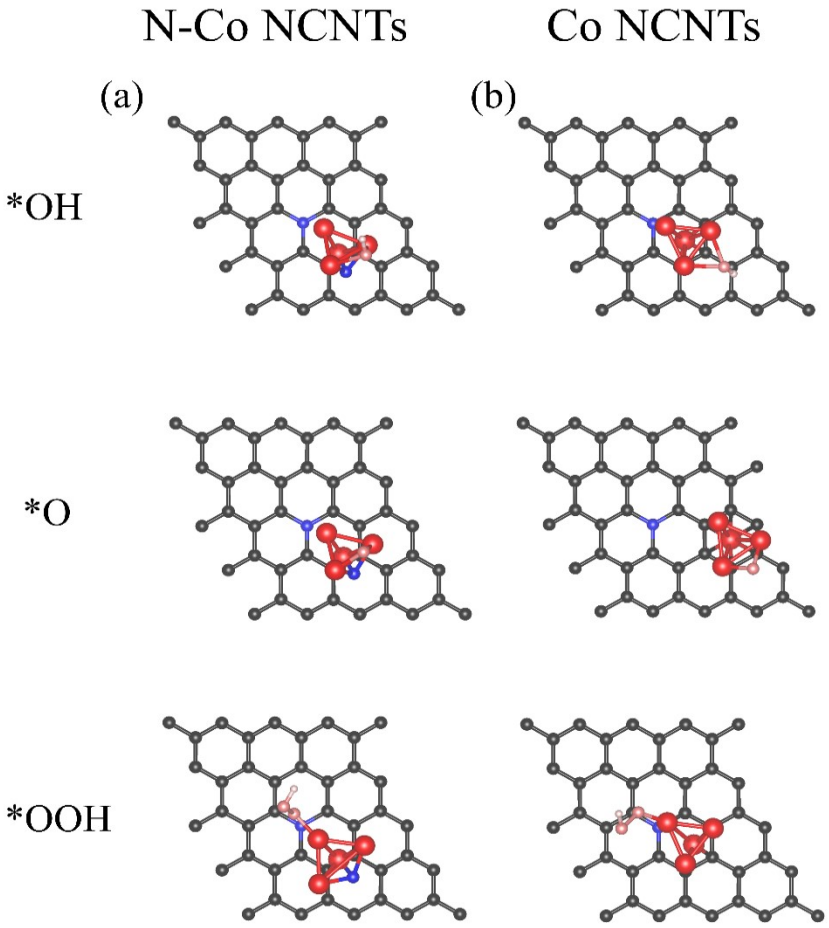

Fig S24. Optimization models for intermediates of N-Co NCNTs (a) and Co NCNTs (b) in OER.

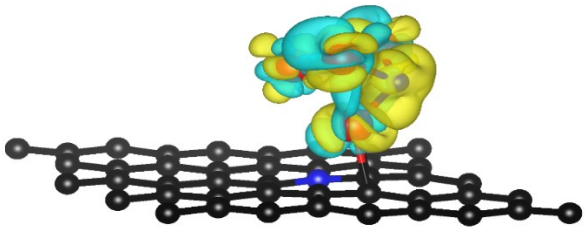

Fig S25. Charge Density difference of N-Co NCNTs.

Table S1. Comparison of the recently-reported cobalt based catalysts for overall water splitting.

Catalysts	Electrolyte (KOH)	η_{10} (V)	Durability (h)	Ref.
N-Co NCNTs|| N-Co NCNTs	1.0	1.53	100	This work
$CoTe_2$/CoP	1.0	1.55	30	[12]
$Co_{5.47}N$/MoN	1.0	1.59	16	[13]
$VCoCO_x$@NF	1.0	1.54	70	[14]
Co/CoO@NC@CC	1.0	1.66	25	[15]
$CoSe_2$/CNTs	1.0	1.75	24	[16]
Part-Ph Co@Co–P@NPCNTs	1.0	1.63	24	[17]
$NiCo_2P_x$/CNTs	1.0	1.61	48	[18]
Co-NCNTFs/NF	1.0	1.62	10	[19]
CoFe@N-CNTs-800	1.0	1.64	20	[20]

References

1 Kresse, G.; Furthmüller, J., *Phys. Rev. B* ***54***, 11169.

2 Kresse, G.; Furthmüller, J., *Comp. Mater. Sci.* ***6***, 15-50.

3 Liu, Y.; Zhang, S.; Jiao, C.; Chen, H.; Wang, G.; Wu, W.; Zhuo, Z.; Mao, J., *Adv. Sci.* 2023**,** ***10***, e2206107.

4 Kattel, S.; Wang, G., *J. Mater. Chem. A* 2013**,** ***1***, 10790.

5 Lin, S.-Y.; Xia, L.-X.; Zhang, L.; Feng, J.-J.; Zhao, Y.; Wang, A.-J., *Chem. Eng. J.* 2021**,** ***424***, 130559.

6 Li, J.; Qian, J.; Chen, X.; Zeng, X.; Li, L.; Ouyang, B.; Kan, E.; Zhang, W., *Compos. Part B Eng.* 2022**,** ***231***, 109573.

7 Zhang, Z.; Li, X.; Zhong, C.; Zhao, N.; Deng, Y.; Han, X.; Hu, W., *Angew. Chem. Int. Ed.* 2020**,** ***59***, 7245-7250.

8 Kitano, S.; Noguchi, T. G.; Nishihara, M.; Kamitani, K.; Sugiyama, T.; Yoshioka, S.; Miwa, T.; Yoshizawa, K.; Staykov, A.; Yamauchi, M., *Adv. Mater.* 2022**,** ***34***, e2110552.

9 NØrskov, J. K.; Rossmeisl, J.; Logadottir, A.; Lindqvist, L.; Kitchin, J. R.; Bligaard, T.; Jonsson, H., *J. Phys. Chem. B* 2004**,** ***108***, 17886−17892.

10 Nie, X.; Luo, W.; Janik, M. J.; Asthagiri, A., *J. Catal.* 2014**,** ***312***, 108-122.

11 Choudhury, P.; Bhethanabotla, V. R.; Stefanakos, E., *J. Phys. Chem. C* 2009**,** ***113***, 13416–13424.

12 Yang, L.; Cao, X.; Wang, X.; Wang, Q.; Jiao, L., *Appl. Catal. B Environ.* 2023**,** ***329***, 122551.

13 Zhu, J.; Du, Q.; Arif Khan, M.; Zhao, H.; Fang, J.; Ye, D.; Zhang, J., *Appl. Surf. Sci.* 2023**,** ***623***, 156989.

14 Meena, A.; Thangavel, P.; Nissimagoudar, A. S.; Narayan Singh, A.; Jana, A.; Sol Jeong, D.; Im, H.; Kim, K. S., *Chem. Eng. J.* 2022**,** ***430***, 132623.

15 Dai, K.; Zhang, N.; Zhang, L.; Yin, L.; Zhao, Y.; Zhang, B., *Chem. Eng. J.* 2021**,** ***414***, 128804.

16 Wei, G.; Du, K.; Zhao, X.; Wang, J.; Yan, W.; An, C.; An, C., *Chin. Chem. Lett.* 2020**,** ***31***, 2641-2644.

17 Jiao, J.; Yang, W.; Pan, Y.; Zhang, C.; Liu, S.; Chen, C.; Wang, D., *Small* 2020**,** ***16***, e2002124.

18 Huang, C.; Ouyang, T.; Zou, Y.; Li, N.; Liu, Z.-Q., *J. Mater. Chem. A* 2018**,** ***6***, 7420-7427.

19 Yuan, Q.; Yu, Y.; Gong, Y.; Bi, X., *ACS Appl. Mater. Interfaces* 2020**,** ***12***, 3592-3602.

20 Guo, P.; Wu, R.; Fei, B.; Liu, J.; Liu, D.; Yan, X.; Pan, H., *J. Mater. Chem. A* 2021**,** ***9***, 21741-21749.